Zhou *et al. Clinical Proteomics* (2026) 23:14
https://doi.org/10.1186/s12014-026-09585-5

Clinical Proteomics

RESEARCH Open Access

Protein corona proteomics characterizes low-abundance plasma protein signatures and highlights ferroptosis-associated signals in uremic hemodialysis patients

Fengying Zhou[1,2,3†], Yaxin Zheng[1,2,3†], Wei Zhang[4†], Ruqi Tan[5], Qi Liao[2], Zhipeng Zeng[3], Guimian Zou[2], Jingsheng Ma[2], Yaoshuang Zou[2], Jinmei Xue[7], Donge Tang[1,2,3*], Yong Dai[2,6,7*] and Huaizhou Chen[2*]

Abstract

Patients with uremia undergoing long-term hemodialysis are prone to multi-organ complications, but the underlying molecular mechanisms remain unclear. Ferroptosis, an iron-dependent form of cell death, has been linked to inflammation and organ damage. Its role in hemodialysis-related pathology, however, has not been well characterized. In this study, we systematically profiled low-abundance plasma proteins from six hemodialysis patients and eight healthy controls using a protein corona–based enrichment technique to enhance detection sensitivity. A total of 183 differentially expressed proteins (DEPs) were defined based on a fold-change threshold (≤ 0.25 or ≥ 4), including 101 upregulated and 82 downregulated proteins. Notably, pathway enrichment analysis highlighted the ferroptosis pathway, with altered abundance of proteins including TFRC, ALOX15, PRNP, CYBB, and ACSL1, suggesting a potential association of ferroptosis-related signals with hemodialysis-related complications. To complement the proteomic analysis, enzyme-linked immunosorbent assay (ELISA) was performed in an independent cohort. ALOX15 showed a significant and reproducible increase in plasma levels ($P < 0.0001$), consistent with the proteomic results. Other ferroptosis-related candidates warrant further evaluation and independent validation in larger cohorts. Furthermore, drug target prediction based on DEP data identified N-oleoyldopamine, luteolin, and catechol as potential compounds targeting the five ferroptosis-related molecules. Collectively, this study provides an exploratory plasma proteomic resource and suggests that ferroptosis-associated plasma protein changes may be relevant to hemodialysis-related complications, warranting further validation. Collectively, this study provides an exploratory plasma proteomic resource and offers initial insights into ferroptosis-associated plasma protein changes in hemodialysis patients.

†Fengying Zhou, Yaxin Zheng and Wei Zhang contributed equally.

*Correspondence:
Donge Tang
donge66@126.com
Yong Dai
daiyong22@aliyun.com
Huaizhou Chen
chz1217@163.com

Full list of author information is available at the end of the article

Keywords Uremia, Hemodialysis, Ferroptosis, Protein corona, Low-abundance proteins

Graphical abstract

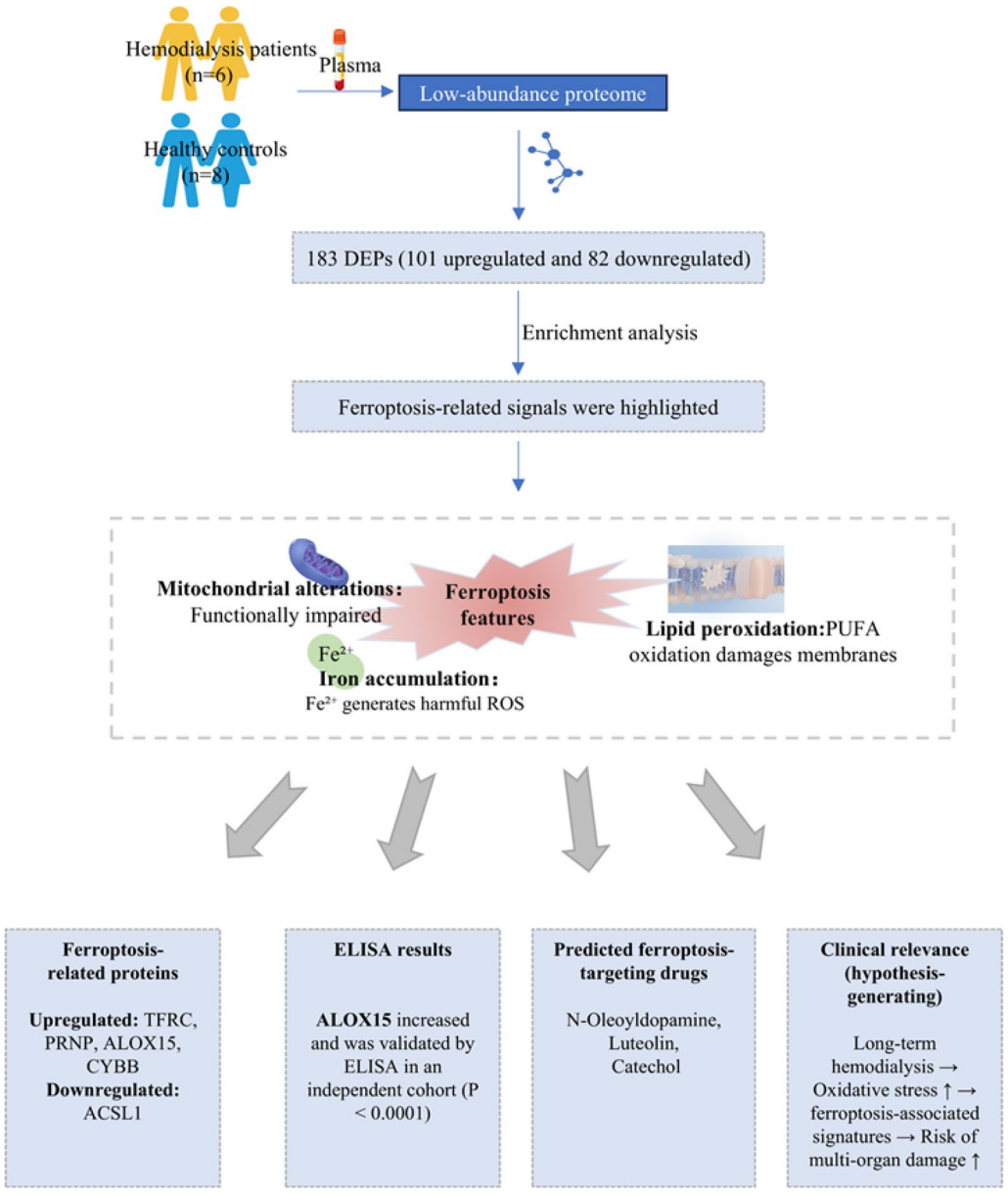

Introduction

Uremia, the clinical manifestation of end-stage renal disease (ESRD), is characterized by the accumulation of metabolic waste, electrolyte imbalances, and hormonal dysregulation [1, 2]. Hemodialysis remains the primary life-sustaining treatment for these patients [3]. However, despite its efficacy in removing toxins, long-term dialysis is associated with a range of complications—particularly cardiovascular, hepatic, and neurological injury—whose underlying molecular mechanisms remain poorly understood [4].

Ferroptosis is a regulated form of cell death driven by iron-dependent lipid peroxidation, and it has emerged as a key mechanism underlying chronic inflammation and tissue injury [5–7]. While ferroptosis has been linked to kidney diseases such as acute kidney injury and renal fibrosis [8–10], its role in long-term hemodialysis patients has not been systematically investigated.

Low-abundance plasma proteins, despite their minimal concentrations, play crucial roles in early pathological signaling and disease progression [11, 12]. However, they are often overlooked due to the masking effect of

high-abundance proteins and the sensitivity limitations of conventional proteomic approaches [13]. Protein corona–based enrichment techniques offer a promising solution by selectively capturing low-abundance proteins, thereby improving detection sensitivity [14].

In this study, we employed an innovative protein corona–based proteomic approach to systematically profile low-abundance plasma proteins in hemodialysis patients and healthy controls. Differentially expressed proteins (DEPs) were defined based on fold-change thresholds and subjected to functional annotation and pathway enrichment analyses to summarize biological patterns and prioritize candidate pathways for follow-up. Ferroptosis-related candidate signals were highlighted, and selected proteins were subsequently quantified using enzyme-linked immunosorbent assay (ELISA) in an independent cohort. In addition, in silico target-based prioritization was performed using the shortlisted ferroptosis-related candidates as input to nominate candidate compounds for future investigation and independent validation.

Materials and methods

Healthy controls and patients

The study was approved by the Medical Ethics Committee of the University of Hong Kong Shenzhen Hospital (2024-096), and informed consent was obtained from all participants. The fundamental clinical characteristics and biochemical parameters of hemodialysis patients are summarized in Table 1. Peripheral blood was collected from 6 hemodialysis patients and 8 HCs for proteomic profiling and for independent ELISA validation (12 hemodialysis patients and 12 HCs). For the hemodialysis patients, blood was drawn into EDTA anticoagulant tubes within one hour prior to the initiation of their hemodialysis session. Similarly, blood from HCs was collected using the same procedure. All collected blood samples were processed within 2 h of collection. They were centrifuged at 1200 × g for 10 min at room temperature. After centrifugation, the upper transparent yellowish plasma layer was carefully aspirated, avoiding the buffy coat and erythrocyte layers. The harvested plasma was then aliquoted into sterile cryovial tubes and immediately frozen at − 80 °C for long-term storage until subsequent analysis.

Table 1 Fundamental clinical characteristics and biochemical parameters in Hemodialysis patients

Variables	Hemodialysis Patients ($n=6$)
Gender (male, %)	66.7
Age (y)	55.8 ± 14.9
ALB (g/L)	35.7 ± 7.1
CREA (μmol/L)	733.8 ± 341.1
UREA (mmol/L)	16.9 ± 10.8
UA (μmol/L)	319.5 ± 90.4
WBC (10^9/L)	7.1 ± 1.9
Hb (g/L)	108.2 ± 19.7
PLT (10^9/L)	197.0 ± 42.1
NEP (%)	66.3 ± 8.6
LYP (%)	17.5 ± 4.7
ALT (U/L)	12.6 (9.8–41.4)
AST (U/L)	14.8 (8.5–39.4)
ALP (U/L)	120.0 (83.0-298.0)
MOP (%)	6.7 (6.0-17.9)

Sample preparation

Low-abundance proteins in plasma were enriched using Proteograph™ assay kit (Seer Inc., Redwood City, CA, USA; https://seer.bio/), which contains five proprietary classes of engineered nanoparticles optimized for protein corona formation and comprehensive plasma proteome coverage [15]. This protein corona strategy leverages affinity-driven adsorption to generate distinct nanoparticle-associated coronas and is designed to expand proteomic coverage and improve the detectability of lower-abundance plasma proteins. The experimental workflow also incorporated a high-abundance protein removal step to reduce dominant plasma components such as albumin and immunoglobulins, thereby enhancing the detection sensitivity for low-abundance proteins. We pooled plasma samples within each group by combining equal volumes from six hemodialysis patients and eight healthy controls, generating two pooled plasma samples representing the patient and HC groups, respectively. The beads were initially dispersed by ultrasonication. A 40 μL aliquot was magnetically separated for 2 min, the supernatant was discarded, and the beads were washed with 100 μL wash buffer under agitation (1300 rpm, 5 min), followed by another magnetic separation. The beads were resuspended in 100 μL wash buffer and mixed with 100 μL plasma, then incubated at 37 °C with shaking (1300 rpm, 1 h). After incubation, the beads were washed three times with 300 μL wash buffer (5 min each). The beads thus obtained were coated with the enriched proteins. The protein-coated beads were resuspended in 40 μL reduction/alkylation buffer, vortexed, and heated at 95 °C (1000 rpm, 5 min), then cooled to room temperature. Proteins were digested with 15 μL protease at 37 °C (1300 rpm, 2 h) and quenched with 3 μL stop reagent. After centrifugation (20,000 g, 1 min), the supernatant was collected. Desalting columns were activated with 100 μL methanol and equilibration buffer (700 g, 1 min), washed twice with 100 μL wash buffer, and peptides were eluted twice with 30 μL elution buffer (700 g, 1 min each). The 60 μL eluate was vacuum-concentrated for mass spectrometry (MS) analysis.

NanoLC-MS/MS analysis

A nano-UPLC system (NanoElute2) coupled with a mass spectrometer (TimsTOF Pro2) was employed to achieve high-resolution separation and sensitive detection of low-abundance peptides. Separation was performed using a reversed-phase column (PePSep C18, 1.9 μm, 75 μm × 15 cm, Bruker, Germany). The mobile phases were 0.1% formic acid in water (A) and 0.1% formic acid in acetonitrile (B). A 60-min gradient was applied: 5–22% B (0–45 min), 22–37% B (45–50 min), 37–80% B (50–55 min), and 80% B (55–60 min). The MS analysis was conducted in a data-independent acquisition (DIA) mode with parallel accumulation-serial fragmentation (PASEF) as the fragmentation method, with a scan range of 400–1201 m/z. Collision energy was dynamically ramped from 20 eV ($1/K_0 = 0.85$ Vs/cm^2) to 59 eV ($1/K_0 = 1.30$ Vs/cm^2), optimizing fragmentation efficiency and improving both the identification and quantification accuracy of low-abundance peptides.

Data retrieval

In this study, raw MS data were analyzed using Spectronaut software (v18.2.230802.50606, Biognosys AG), and database searches were performed using the integrated Pulsar engine. Spectra were searched against species-specific entries in the UniProt FASTA database (uniprot_Homo sapiens_9606_reviewed_2023_09. fasta). The following three modifications are to be considered: carbamidomethyl [C] as a fixed modification, oxidation (M) and acetyl (Protein N-term) as variable modifications. Trypsin was used as the proteolytic enzyme, allowing up to two missed cleavage sites. Both precursor and fragment mass tolerances were set to 20 ppm and were used for mass recalibration. The false discovery rate (FDR) for peptide identification was strictly controlled at 1% at both the peptide-spectrum match (PSM) and peptide levels. LC–MS data were acquired under identical LC gradients, instrument settings, and reagent lots. Eleven indexed retention time (iRT) standard peptides were spiked in to facilitate retention time alignment and ensure chromatographic quality control. Proteins were filtered based on the number of unique peptides, retaining only those with at least one unique peptide. For DIA data, missing values were imputed using the half-minimum method to ensure consistent and reasonable handling of missing values across samples. All quantitative data were $\log_2$-transformed and center-scaled using R (v3.6.3). DEPs were defined based on stringent fold-change thresholds (≥ 4 for upregulation and ≤ 0.25 for downregulation).

Enrichment analysis

Homology classification was performed using the KOG database (http://www.ncbi.nlm.nih.gov/COG/) to summ arize the functional categories of the identified proteins. Subcellular localization prediction was conducted to determine the potential cellular distribution of the identified proteins. Subcellular localization was predicted using the CELLO online tool (http://cello.life.nctu.edu.tw/). Protein identifiers were converted to gene symbols using BLAST and subsequently mapped to Gene Ontology (GO) terms for Homo sapiens. GO enrichment analysis covered cellular components (CCs), molecular functions (MFs), and biological processes (BPs), using the GO database (http://www.geneontology.org/). Pathway analysis of DEPs was performed using the Kyoto Encyclopedia of Genes and Genomes (KEGG) database (https://www.kegg.jp/kegg/pathway.html). For both GO and KEGG analyses, the list of DEPs was used as the input, and all identified proteins in the current proteomic dataset were used as the background reference set, ensuring enrichment was evaluated within the experimental detection scope. GO and KEGG enrichments were evaluated for statistical significance using Fisher's exact test. Final visualization of GO and KEGG was plotted by https://www.bioinformatics.com.cn (last accessed on 1st April 2025).

Protein-protein interaction (PPI) network construction and key subnets identification

PPI network was generated using the STRING database (https://cn.string-db.org), with a confidence score of 0.4 set as the minimum required interaction threshold, while all other parameters remained at default levels [16]. The resulting network was visualized using Cytoscape software (version 3.10.2) [17], and the key subnets were extracted using the MCODE plugin.

Hub proteins screening

To identify key regulatory proteins within the PPI network, we used the cytoHubba plugin in Cytoscape and applied the Maximal Clique Centrality (MCC) algorithm to rank network nodes. The top seven hub proteins with the highest scores were selected.

ELISA

The ELISA was performed on newly collected plasma samples obtained from both hemodialysis patients and HCs following the manufacturers' protocols. The assay kits used were: TFR1 (Chengdu Yuannuo-Tiancheng Technology Co., Ltd., Cat# YMS10440-A), ACSL1 (Chengdu YuannuoTiancheng Technology Co., Ltd., Cat# YMS10077-A), ALOX15 (Chengdu YuannuoTiancheng Technology Co., Ltd., Cat# YNL-15913), PRNP (ZOKEYO, Cat# Y-92092) and CYBb (Bioswamp, Cat# HM13087).

Drug prediction

To identify potential therapeutic compounds targeting ferroptosis-related proteins, drug-gene interaction

analysis was performed using the Drug Signature Database (DSigDB) via the Enrichr platform (https://maayanlab.cloud/Enrichr/). DSigDB is a comprehensive resource that integrates experimentally validated drug–gene associations and transcriptional response signatures, enabling systematic prediction of compounds potentially linked to the observed protein changes. This resource comprises 22,527 gene sets and 17,389 unique compounds across 19,531 genes [18]. The list of ferroptosis-related proteins shortlisted from the DEP set was used as input, and candidate compounds were ranked based on adjusted P-values. Compounds with an adjusted P-value < 0.01 were prioritized for reporting.

Statistical analysis

Data analysis was performed with the IBM SPSS Statistics 27 (IBM Corp., Armonk, NY), and the results was displayed with the GraphPad Prism, version 10.1.2 (GraphPad Software, La Jolla, CA). Variables were tested for normality using Shapiro-Wilk test. Normally distributed data were presented as mean ± standard deviation (SD) and analyzed by independent t-test; non-normally distributed data were expressed as median (interquartile range, IQR) and analyzed by Mann-Whitney U test. A two-tailed $P < 0.05$ was considered statistically significant ($^{*}P < 0.05$; $^{**}P < 0.01$; $^{***}P < 0.001$; $^{****}P < 0.0001$).

Results

Substantial alterations in low-abundance plasma proteins between hemodialysis patients and HCs

This study employed protein corona proteomics to systematically profile the low-abundance plasma proteome in uremic hemodialysis patients. The overall workflow is illustrated (Fig. 1A), including sample preparation, MS analysis, and subsequent bioinformatics processing. The base peak chromatogram (BPC) and total ion chromatogram (TIC) demonstrated strong and consistent signal intensities with well-distributed peaks, indicating high-quality and reliable MS performance (Fig. 1B). A total of 183 DEPs were identified between hemodialysis patients and HCs using a stringent fold-change threshold (≤ 0.25 or ≥ 4), representing 8.0% of the 2,085 proteins quantified. Of these DEPs, 101 were upregulated and 82 were downregulated in hemodialysis patients (Fig. 1C and D). The top 10 most significantly upregulated and downregulated DEPs were further highlighted (Fig. 1E).

Functional categorization of low-abundance deps indicates enrichment in signaling, cytoskeletal regulation, and protein homeostasis

To gain further insight into the biological roles of the DEPs, we performed KOG functional classification analysis. The results revealed that these DEPs were distributed across diverse functional categories. The corresponding bar chart shows that most proteins were enriched in signal transduction mechanisms (27 proteins), cytoskeleton (17 proteins), general function prediction (15 proteins), and posttranslational modification, protein turnover, and chaperones (10 proteins) (Fig. 2A). These findings suggest that dysregulation of signaling pathways, cytoskeletal dynamics, and protein quality control may underlie the pathological changes associated with long-term hemodialysis—processes that are uniquely reflected by alterations in low-abundance plasma proteins.

Low-abundance deps are predominantly localized to the cytoplasm, extracellular space, and nucleus

Subcellular localization prediction was conducted to determine the potential cellular distribution of the identified proteins. Subcellular localization analysis indicated that the majority of DEPs were localized in the cytoplasm (58 proteins, 31.69%), secreted (56 proteins, 30.60%), and nucleus (47 proteins, 25.68%). Fewer proteins were distributed in the plasma membrane (9 proteins, 4.92%), mitochondrion (6 proteins, 3.28%), peroxisome (2 proteins, 1.09%), and endoplasmic reticulum membrane (2 proteins, 1.09%) (Fig. 2B). These results imply that the identified DEPs are mainly involved in intracellular signaling, secretion, and nuclear functions, underscoring their relevance to the altered microenvironment in hemodialysis patients.

Ferroptosis-associated signatures highlighted in the plasma proteome of hemodialysis patients

To explore the biological roles of DEPs, GO and KEGG enrichment analyses were performed. In the BP category, DEPs were enriched in immune system processes, metal ion response, and stress response, reflecting patterns potentially related to oxidative stress adaptation and iron metabolism dysregulation—both hallmarks of ferroptosis (Fig. 3A). Enrichment in xenobiotic response, leukocyte activation, and lipid transport further suggests involvement in inflammatory and lipid metabolic processes.

In the MF category, DEPs were enriched in antigen, RNA, and protein binding, as well as insulin-like growth factor II binding, indicating roles in immune signaling and molecular recognition. Additional terms related to lipopolysaccharide binding, receptor interaction, and calcium ion binding suggest participation in ferroptosis-related inflammatory and oxidative signaling (Fig. 3B).

For the CC category, DEPs were mainly localized to extracellular regions, vesicles, and exosomes, implying functions in intercellular communication and immune modulation. Enrichment in cytoplasmic and secretory vesicle lumens and the phagocytic compartment further is consistent with roles in innate immunity. Notably, the presence of DEPs in the HFE–transferrin receptor complex and mitochondrial nucleoid relates to iron

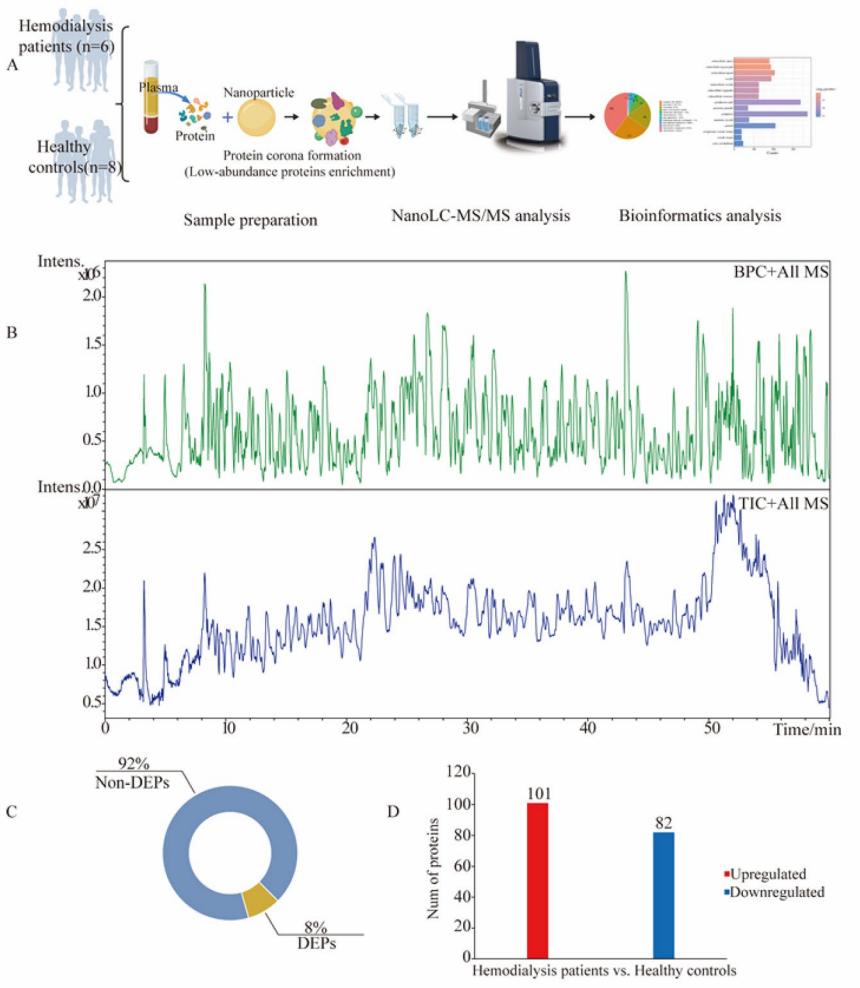

E

Number	Upregulated			Downregulated		
	Protein accession	Gene name	Fold change	Protein accession	Gene name	Fold change
1	P00709	LALBA	629.6412044	P00966	ASS1	0.248914226
2	Q9GZU2	PEG3	503.7403624	Q15311	RALBP1	0.245938081
3	P48788	TNNI2	410.8506787	A0A0A0MT36	IGKV6D-21	0.243533805
4	P45378	TNNT3	283.6932001	P68363	TUBA1B	0.240441945
5	O60264	SMARCA5	274.5254848	Q9NQC3	RTN4	0.238360683
6	Q96A32	MYL11	229.0215291	Q9UJC5	SH3BGRL2	0.235705991
7	A0A0C4DH24	IGKV6-21	217.2042701	Q9Y2I8	WDR37	0.22429215
8	P51511	MMP15	193.5342184	A0A075B6R2	IGHV4-4	0.221264559
9	Q8NES3	LFNG	150.4653444	P15259	PGAM2	0.217343623
10	P13164	IFITM1	148.0229835	Q9P0L0	VAPA	0.214979911

Fig. 1 Experimental Workflow and Quantitative Profiling of DEPs. (**A**) Experimental workflow: Plasma samples from six hemodialysis patients and eight HCs were subjected to protein corona formation using nanomaterials to enrich low-abundance proteins. The illustration depicts the principle of protein corona formation, where plasma proteins adsorb onto the nanoparticle surface according to their physicochemical affinities, enabling selective enrichment of low-abundance proteins while reducing interference from high-abundance species. The enriched samples were analyzed by nanoLC-MS/MS, followed by bioinformatics analysis to identify and characterize DEPs and their functional pathways; (**B**) Base peak chromatogram (BPC) and total ion chromatogram (TIC) of all detected peptides, showing retention time (minutes) and intensity; (**C**) Proportion of DEPs among total identified proteins: DEPs accounted for 8%, and the remaining 92% were non-DEPs; (**D**) Number of DEPs identified in hemodialysis vs. HCs: 101 proteins were upregulated, and 82 were downregulated in hemodialysis patients; (**E**) Top 10 DEPs ranked by fold change, including upregulated proteins (e.g., LALBA, PEG3) and downregulated proteins (e.g., ASS1, RALBP1), with UniProt accession numbers, gene names, and fold changes

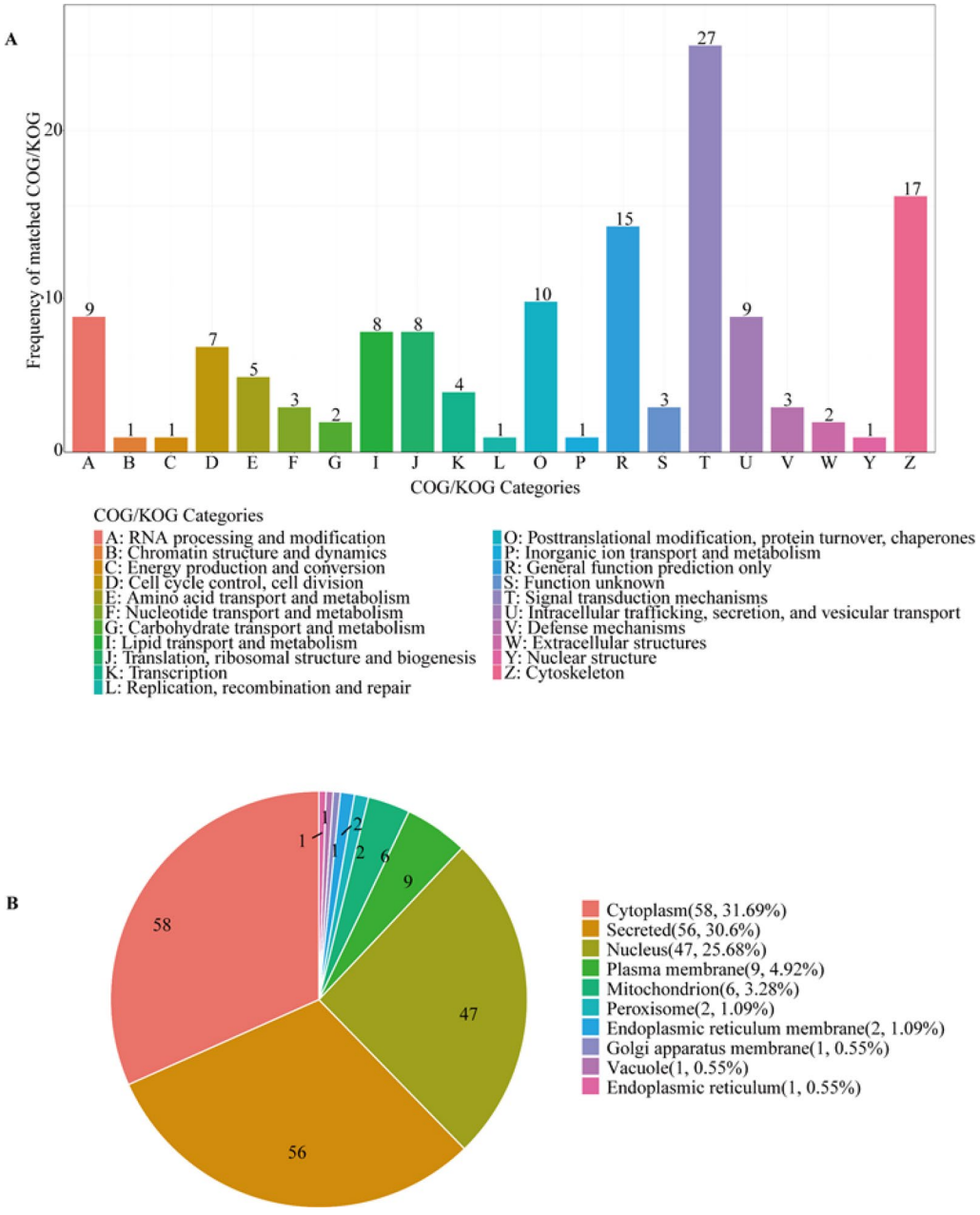

Fig. 2 Functional Categorization and Subcellular Localization of DEPs. (**A**) The bar plot shows COG/KOG-based functional classification of DEPs. Major categories include RNA processing and modification (**A**), chromatin structure and dynamics (**B**), amino acid transport and metabolism (E), transcription (K), among others; (**B**) The pie chart shows subcellular localization of DEPs, with the majority located in the cytoplasm (31.69%), secreted (30.6%), and nucleus (25.68%). Minor localizations include mitochondria (3.28%), plasma membrane (4.92%), and other organelles

metabolism and mitochondrial processes that are often implicated in ferroptosis-related biology (Fig. 3C).

Notably, the KEGG pathway analysis highlighted enrichment of the ferroptosis pathway, suggesting that ferroptosis-related signals may be associated with the pathophysiology of uremia in hemodialysis patients. This pathway is characterized by lipid peroxide accumulation, underscoring the importance of oxidative stress and iron dysregulation in disease progression, consistent with our prior findings. Specifically, ferroptosis-related proteins such as TFRC, PRNP, ALOX15, ACSL1, and CYBB were identified among the DEPs in patient plasma, highlighting ferroptosis-related candidate signals for further evaluation. These results prioritize these proteins for follow-up validation in independent cohorts (Fig. 3D). To explore the interactions among the DEPs, we constructed and visualized a PPI network. The analysis identified seven top hub proteins, including SNRPA1, SF3A1,

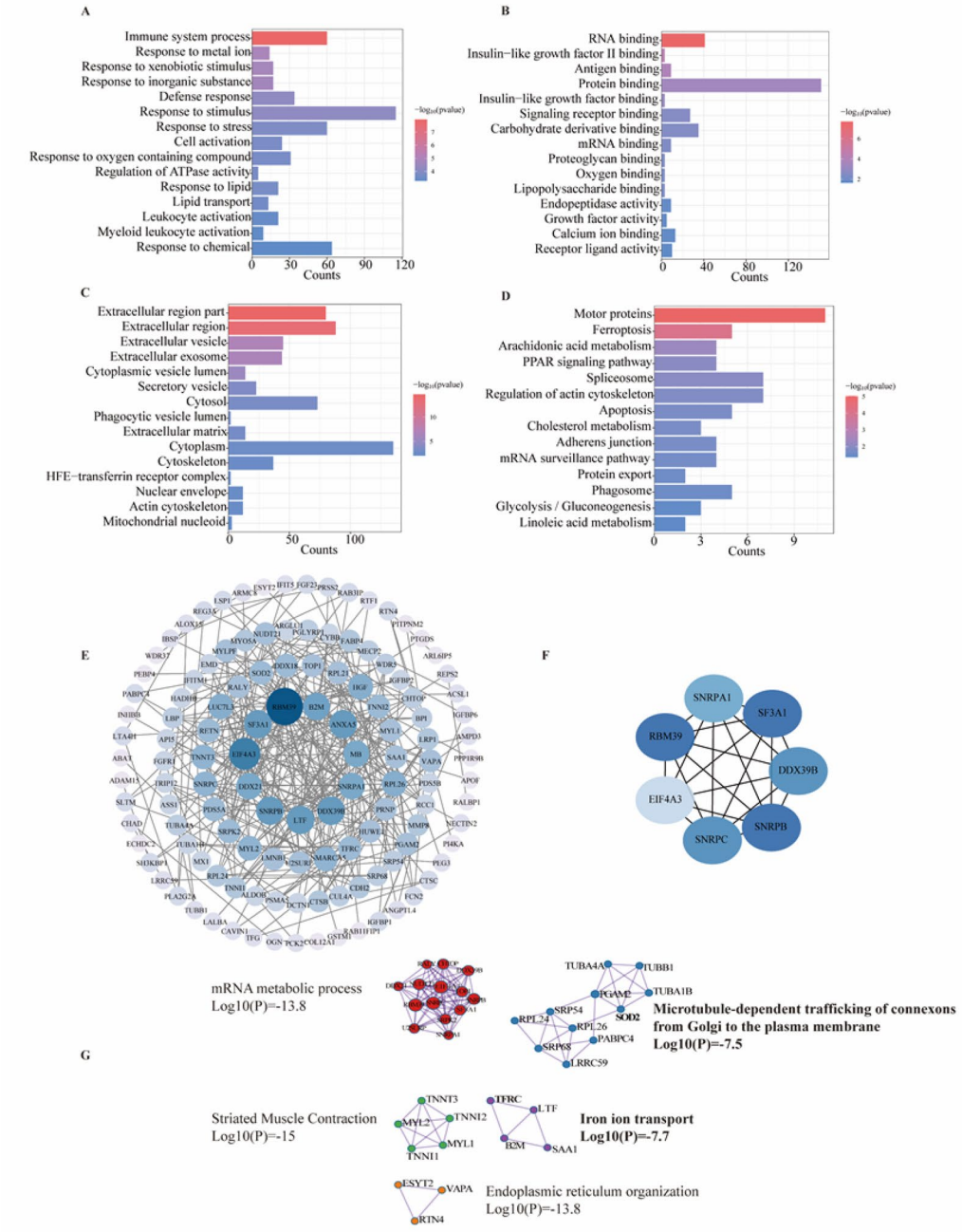

Fig. 3 Functional Annotation and Network Analysis of DEPs. (**A**) GO-BP enrichment analysis revealed involvement in immune-related processes, metal ion response, xenobiotic stimulus response, and defense response; (**B**) GO-MF enrichment showed that proteins are mainly associated with insulin-like growth factor binding, signaling receptor binding, mRNA binding, and calcium ion binding; (**C**) GO-CC enrichment analysis indicated that proteins are predominantly localized in the extracellular region, cytoplasm, and nuclear envelope; (**D**) KEGG analysis highlighted pathways including ferroptosis, arachidonic acid metabolism, PPAR signaling, spliceosome, and apoptosis; (**E**) PPI network of DEPs. (**F**) The top 7 hub proteins were identified based on network topology. (**G**) MCODE analysis revealed several highly interconnected functional modules, including SRP-mediated translational regulation, SOD2-dependent oxidative stress response, and TFRC-mediated iron ion transport. The ferroptosis-related subnetwork was highlighted in bold to improve interpretability and emphasize its biological relevance within the global PPI network

and EIF4A3, which exhibited high connectivity, indicating that they occupy central positions in the network topology (Fig. 3E and F). Subsequent functional clustering analysis revealed several distinct biological modules, including mRNA metabolic processes, striated muscle contraction, iron ion transport, and endoplasmic reticulum organization. Notably, the cluster containing TFRC and LTF was annotated with iron ion transport–related terms, and TFRC is also a ferroptosis-related protein identified among the DEPs. Additionally, SOD2 and its interacting partners may be involved in maintaining redox homeostasis through microtubule-associated trafficking. Together, these network features and functional modules provide an overview of coordinated protein changes and highlight iron transport and redox-related clusters for further investigation (Fig. 3G).

A hypothesis-generating model linking ferroptosis-associated signatures with ROS generation and lipid metabolism in hemodialysis patients

Given the enrichment of the ferroptosis pathway among low-abundance proteins in the above analysis and its known involvement in iron-dependent oxidative injury, we further examined ferroptosis for its potential relevance to hemodialysis-associated alterations. Firstly, five ferroptosis-related proteins were defined as DEPs based on fold-change threshold in our study: TFRC, ALOX15, PRNP, CYBB, and ACSL1 (Fig. 4A). Second, a focused PPI subnetwork was constructed to contextualize the ferroptosis-related proteins within their potential regulatory environment. This subnetwork was extracted from the global PPI network by selecting proteins that showed the strongest interactions with the five ferroptosis-related proteins. The resulting local interaction network indicates close connectivity between these ferroptosis-related proteins and multiple functional partners, providing groundwork for subsequent investigation into their potential involvement in the pathophysiology of hemodialysis (Fig. 4B).

Drawing on established mechanistic knowledge of ferroptosis from the literature, we present a conceptual schematic of how these signals could potentially converge in hemodialysis patients (Fig. 4C). In this model, TFRC may contribute to iron uptake, while CYBB (a component of NADPH oxidase) may be linked to reactive oxygen species (ROS) production. Elevated ROS, together with iron-dependent reactions (Fenton reaction), may promote oxidative stress, which could influence lipid peroxidation pathways involving ALOX15 and facilitate the generation of phospholipid hydroperoxides (PLOOHs), a biochemical feature compatible with ferroptosis. Reduced ACSL1 abundance may, conversely, decrease the availability of lipid substrates and thereby potentially attenuate lipid peroxidation processes. Collectively, this model provides a literature-informed framework for future mechanistic experiments and individual-level validation.

ELISA quantification supports upregulation of the ferroptosis-related protein ALOX15 in hemodialysis patients

To supplement the proteomic findings, we performed ELISA assays to quantify the plasma levels of five ferroptosis-related proteins in an independent cohort of 12 hemodialysis patients and 12 HCs (Fig. 4D). Among these, ALOX15 levels were significantly elevated in the hemodialysis group (64.07 ng/mL vs. 28.16 ng/mL, $P < 0.0001$), in line with the proteomic trend. However, TFRC, PRNP, CYBB, and ACSL1 did not show statistically significant differences. Protein corona proteomics employs nanoparticles to enrich low-abundance proteins, coupled with high-resolution mass spectrometry, enabling the detection of proteins that may not be captured by ELISA due to antibody specificity or sample complexity. These two platforms are based on different principles and offer complementary insights.

Drug prediction analysis identifies N-oleoyldopamine, luteolin, and catechol as candidate compounds linked to ferroptosis-related proteins

To prioritize candidate compounds potentially linked to ferroptosis-related protein changes in hemodialysis patients, we performed drug prediction analysis using the DSigDB via the Enrichr platform. DSigDB is a comprehensive resource that integrates experimentally validated drug–gene associations and transcriptional response signatures, enabling systematic prediction of compounds potentially linked to the observed protein changes. Based on the five ferroptosis-related DEPs (TFRC, ALOX15, PRNP, CYBB, and ACSL1), the top 10 candidate compounds were ranked by adjusted P-values (Fig. 5A). Notably, N-Oleoyldopamine (CTD 00004334), Luteolin (TTD 00009051), and Catechol (CTD 00001636) were prioritized because they were linked to multiple target proteins, supporting their prioritization as candidate compounds for follow-up investigation. The compound–target interactions are illustrated (Fig. 5B), while detailed pharmacological properties, including chemical structures and molecular formulas, are summarized (Fig. 5C). Collectively, these results nominate hypothesis-generating compounds for future validation in experimental models.

Discussion

In this study, we employed the protein corona proteomics technique to systematically analyze plasma samples from patients undergoing hemodialysis due to uremia. This approach successfully enriched a wide range of low-abundance proteins and identified a distinct set of DEPs.

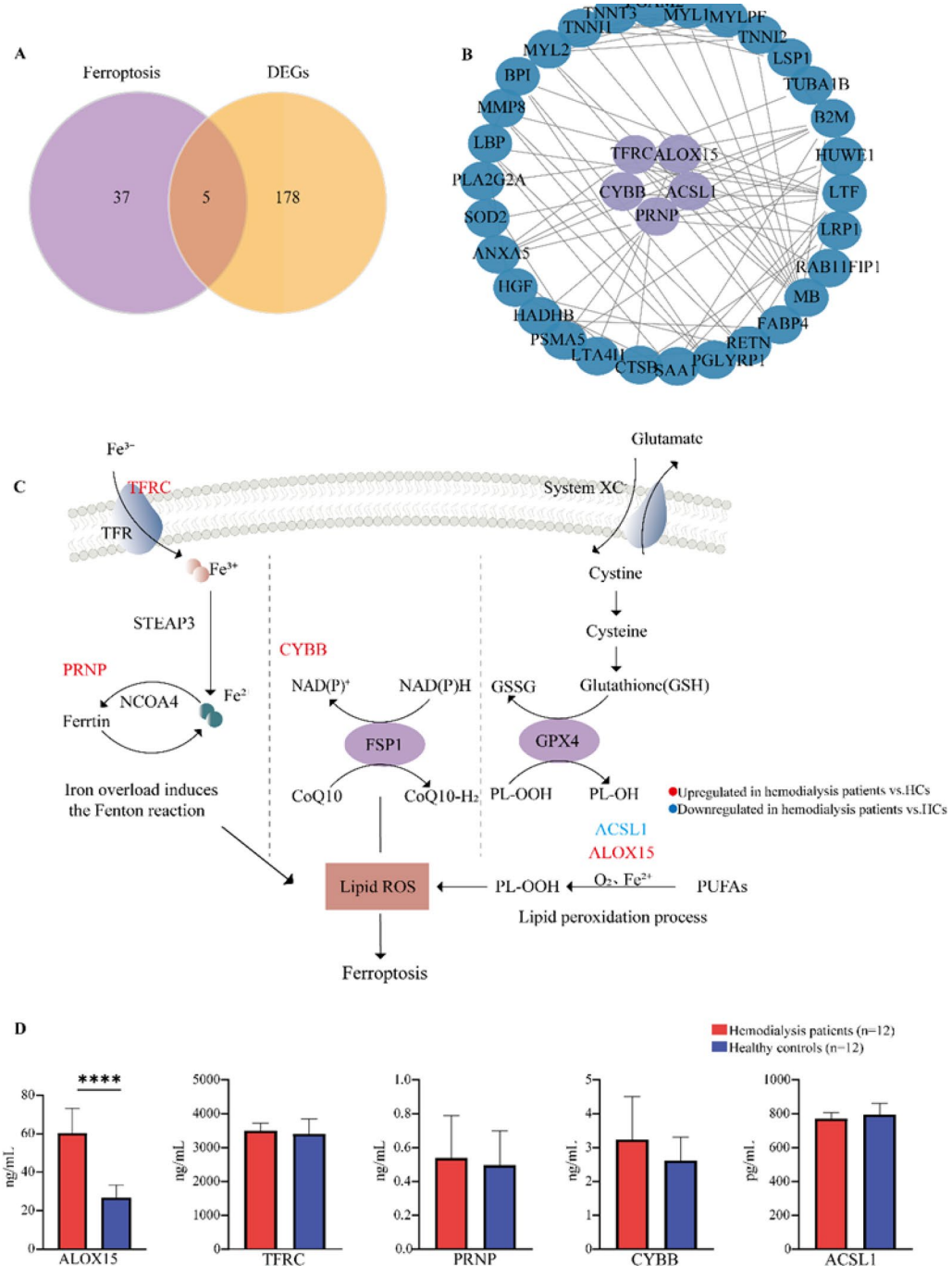

Fig. 4 Ferroptosis Analysis and ELISA Validation. (**A**) Intersection analysis of ferroptosis-related pathways and DEPs: The venn diagram highlights 5 proteins enriched in ferroptosis pathway; (**B**) Focused PPI subnetwork of five ferroptosis-related proteins (TFRC, ALOX15, CYBB, PRNP, and ACSL1), the network was extracted from the global PPI network by selecting the most strongly interacting proteins; (**C**) Schematic of ferroptosis mechanism with protein localization: ferroptosis is a regulated form of cell death characterized by iron accumulation and lipid peroxidation. Its core mechanisms involve dysregulated iron metabolism leading to ROS generation, the FSP1-CoQ10-NAD(P)H axis that counteracts lipid peroxidation, and the classical glutathione-GPX4 antioxidant defense pathway. In this study, five ferroptosis-related DEPs (TFRC, PRNP, CYBB, ALOX15, and ACSL1) were identified and mapped to key regulatory nodes within the pathway. Among them, TFRC, PRNP, CYBB, and ALOX15 were upregulated in the hemodialysis group, whereas ACSL1 was downregulated. This schematic is intended for hypothesis generation and does not constitute mechanistic evidence from the current dataset. (**D**) ELISA validation results, hemodialysis group ($n = 12$) vs. HC group ($n = 12$)): ALOX15 expression was upregulated in the hemodialysis group ($P < 0.0001$), showing consistency with the proteomic trend for ALOX15. The other four proteins (TFRC, ACSL1, PRNP, and CYBB) did not show statistically significant differences by ELISA

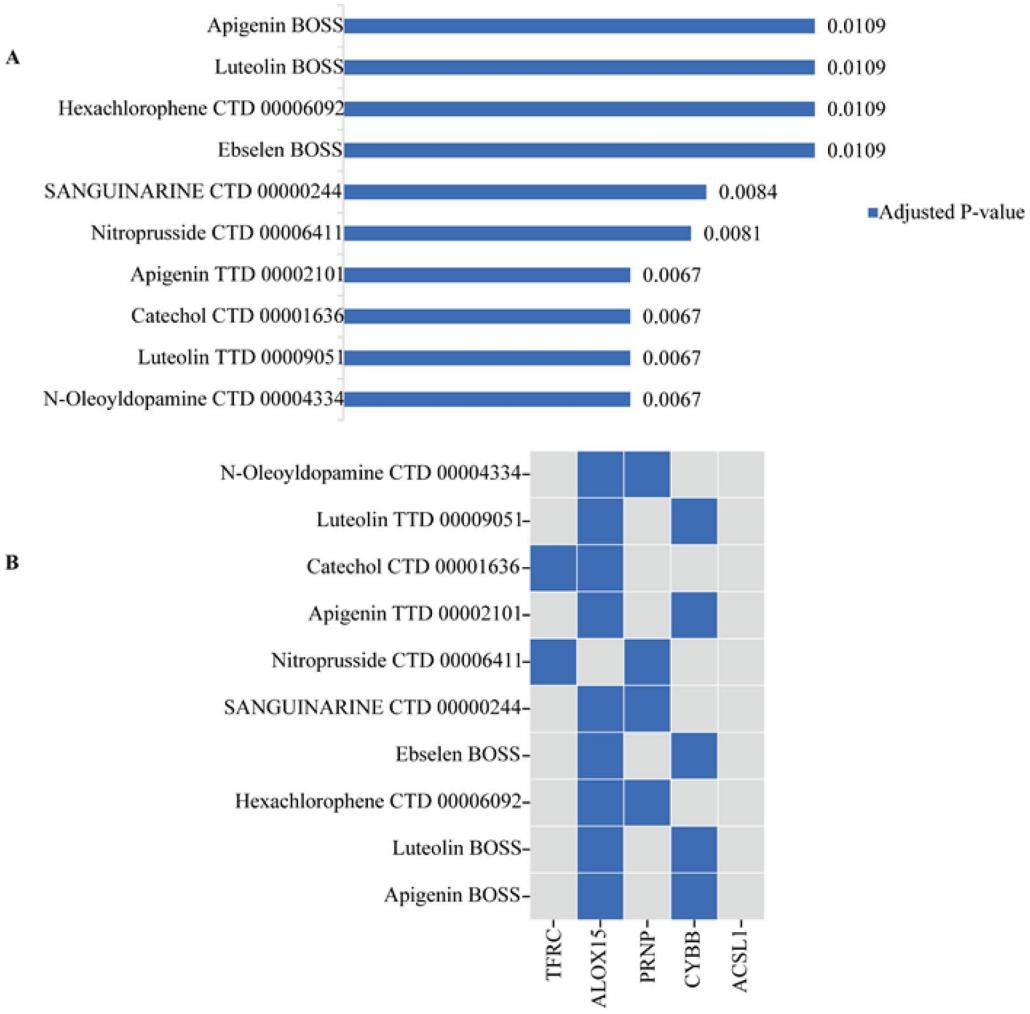

C

Drug names	P-value	Adjusted P-value	Genes	Molecular Formula	Structure
N-Oleoyldopamine CTD 00004334	< 0.0001	0.0067	PRNP; ALOX15	$C_{26}H_{43}NO_3$	
Luteolin TTD 00009051	< 0.0001	0.0067	ALOX15; CYBB	$C_{15}H_{10}O_6$	
Catechol CTD 00001636	0.0001	0.0067	TFRC; ALOX15	$C_6H_6O_2$	
Apigenin TTD 00002101	0.0001	0.0067	ALOX15; CYBB	$C_{15}H_{10}O_5$	
Nitroprusside CTD 00006411	0.0001	0.0081	PRNP; TFRC	$C_5FeN_6O^{-2}$	
SANGUINARINE CTD 00000244	0.0001	0.0084	PRNP; ALOX15	$C_{20}H_{14}NO^{4+}$	
Ebselen BOSS	0.0002	0.0109	ALOX15; CYBB	$C_{13}H_9NOSe$	
Hexachlorophene CTD 00006092	0.0002	0.0109	PRNP; ALOX15	$C_{13}H_6Cl_6O_2$	
Luteolin BOSS	0.0002	0.0109	ALOX15; CYBB	$C_{15}H_{10}O_6$	
Apigenin BOSS	0.0002	0.0109	ALOX15; CYBB	$C_{15}H_{10}O_5$	

Fig. 5 Drugs Prediction Analysis for 5 Ferroptosis-Related Genes. (**A**) Top 10 candidate drugs ranked by P-value the via Enrichr platform (DSigDB database): Key compounds include apigenin, luteolin, hexachlorophene, etc., annotated with data sources (e.g., BOSS, CTD) and P-values; (**B**) Interaction network between the top 10 drugs and 5 ferroptosis-related proteins: Highlights functional associations between drugs (e.g., N-oleoyldopamine) and proteins (e.g., ALOX15, PRNP, CYBB); (**C**) Drug information table: Lists P-values, adjusted P-values, targeted genes, molecular formulas, and structures

Enrichment analyses highlighted ferroptosis-related signals, which may be relevant to hemodialysis-associated molecular alterations. By integrating the DEPs with a ferroptosis-related gene database, we identified five ferroptosis-related DEPs—TFRC, ALOX15, PRNP, CYBB, and ACSL1—that warrant further evaluation in independent cohorts. Among these, ALOX15 showed a reproducible increase in patient plasma and was confirmed by ELISA, supporting its potential utility as a candidate marker associated with ferroptosis-related biology.

Taken together, enrichment patterns and candidate mapping point to a possible convergence of multiple biological processes. GO enrichment analysis indicated that DEPs were broadly involved in iron homeostasis, oxidative stress responses, and lipid metabolism—three central processes in the initiation and amplification of ferroptosis [19, 20]. Specifically, TFRC mediates cellular iron uptake [21, 22], CYBB regulates NADPH oxidase activity and promotes ROS production [23, 24], and ALOX15 catalyzes the peroxidation of PUFAs [25–27]. Notably, ALOX15 has also been implicated in redox regulation and inflammatory signaling, supporting its broader contribution to oxidative injury [28, 29]. In parallel, PRNP and ACSL1 participate in metal ion binding and fatty acid esterification, respectively [30, 31], linking these candidates to pathways related to iron handling and lipid metabolism. Importantly, we observed a downregulation of ACSL1, which may reflect a compensatory response to limit PUFA biosynthesis and attenuate lipid peroxidation-induced damage [32]. Together, these observations provide a literature-informed framework for understanding how iron metabolism, ROS generation, and lipid peroxidation pathways may intersect with ferroptosis-related candidate signals in uremic hemodialysis patients, but require independent validation and mechanistic testing.

Among the ferroptosis-related regulators, ALOX15 emerged as a prioritized candidate due to its established role in lipid peroxidation. Its reproducible elevation in patient plasma, validated by ELISA, supports ALOX15 as a candidate node for follow-up investigation associated with ferroptosis-related biology in hemodialysis patients. Moreover, drug prediction analyses using the DSigDB database nominated pharmacological modulators linked to ALOX15, including natural compounds such as N-oleoyldopamine, luteolin, apigenin, and catechol, which are known for their antioxidant and lipid-modulating properties [33–38]. Together, these findings prioritize ALOX15 and its associated compounds for future experimental validation. If further validated in mechanistic studies and independent clinical cohorts, ALOX15 may represent a candidate intervention-relevant node for follow-up investigation in uremia-related complications. To further examine the expression trends of ferroptosis-related DEPs, we performed ELISA to quantify the levels of TFRC, ALOX15, CYBB, PRNP, and ACSL1 in patient and control plasma. While ALOX15 showed consistent upregulation in both proteomic and ELISA data, the other proteins did not show consistent or statistically significant differences in this cohort. This discrepancy may reflect the methodological differences between the two approaches: MS-based protein corona analysis primarily reflects the relative abundance of peptide fragments adsorbed onto nanoparticle surfaces, whereas ELISA quantifies total immunoreactive protein, which may include distinct isoforms or modified variants not captured by MS-based quantification [39]. These platforms therefore capture related but not identical molecular readouts. Furthermore, factors such as protein conformation, antibody specificity, assay sensitivity, and inter-individual variability may also contribute to the inconsistent findings.

This study has several limitations. The cohort size was relatively small, and the proteomics stage used pooled plasma samples, which limited assessment of inter-individual variability. Second, the protein corona–based enrichment workflow improves the detection and coverage of low-abundance plasma proteins. As a result, the observed proteomic profile may preferentially reflect changes in proteins captured by the nanoparticle corona and may underrepresent alterations in highly abundant plasma proteins. Future studies incorporating complementary proteomic strategies will help to provide a more comprehensive view of the plasma proteome in hemodialysis patients. Third, although ferroptosis-related signals were highlighted in the enrichment analyses, plasma biochemical indicators relevant to ferroptosis (e.g., iron, ferritin, and lipid peroxidation markers) were not assessed in the current study. Integrating these biochemical measurements in future studies will strengthen biological interpretation and facilitate mechanistic validation. To address these limitations, future work will incorporate larger individual-level cohorts and apply targeted quantitative validation approaches (e.g., PRM) alongside ferroptosis-relevant biochemical assessments, together with multi-omics integration where feasible.

Conclusion

In this exploratory study, protein corona proteomics enabled systematic profiling of low-abundance plasma protein alterations in uremic hemodialysis patients. These data provide a low-abundance plasma proteomic resource and nominate ferroptosis-associated candidate signals, including ALOX15, for future validation and mechanistic investigation.

Author contributions

Study concept and design: FYZ, DET, WZ, RQT and YD. Research sample collecting: FYZ, YXZ and RQT. Acquisition of data: ZPZ, RQT, GMZ and YSZ.

Analysis and interpretation of data: JSM, YSZ, JMX and YXZ. Statistical analysis: ZPZ, JSM and YSZ. Drafting of the manuscript: FYZ, WZ and YXZ. Critical revision and final approval of the manuscript: WZ, YD, DET and HZC. Study supervision: YD, HZC and DET. All authors contributed to the article and approved the submitted version.

Funding
This study was supported by the Shenzhen Science and Technology Program (GJHZ20220913142614027), Taizhou Science and Technology Bureau (23ywa60), Science and Technology Plan of Guilin (20220139-1-1), Guangxi Natural Science Foundation (2024GXNSFAA010301), Shenzhen High-level Hospital Construction Fund, and Peking University Shenzhen Hospital Scientific Research Fund (KYQD2024431).

Data availability
The proteomics datasets generated in this study are available at OMIX under the accession number OMIX010821 (https://ngdc.cncb.ac.cn/omix/preview/JodPhOZz).

Declarations

Ethics approval and consent to participate
The study was approved by the Medical Ethics Committee of the University of Hong Kong Shenzhen Hospital (2024-096).

Competing interests
The authors declare no competing interests.

Author details
[1]College of Life Sciences, Guangxi Normal University, Guilin 541006, Guangxi, China
[2]Department of Organ Transplantation, The 924th Hospital of the Chinese People's Liberation Army Joint Logistic Support Force, Guilin 541002, Guangxi, China
[3]Clinical Medical Research Center, Shenzhen People's Hospital (The First Affiliated Hospital, Southern University of Science and Technology; The Second Clinical Medical College, Jinan University), Shenzhen 518020, Guangdong, China
[4]Department of Clinical Laboratory, Peking University Shenzhen Hospital, Shenzhen 518036, Guangdong, China
[5]Department of Nephrology, The University of Hong Kong-Shenzhen Hospital, Shenzhen 518053, Guangdong, China
[6]School of Medicine, Anhui University of Science & Technology, Huainan 232001, Anhui, China
[7]Comprehensive Health Industry Research Center, Southern University of Science and Technology Taizhou Research Institute, Taizhou 318000, Zhe Jiang, China

Received: 12 September 2025 / Accepted: 25 January 2026
Published online: 08 February 2026

References

1. Lyu D, He G, Zhou K, et al. Identification of Immune-Related genes as biomarkers for uremia [J]. Int J Gen Med. 2023;16:5633–49.
2. Wong HS, Chang CM, Kao CC, et al. V-J combinations of T-cell receptor predict responses to erythropoietin in end-stage renal disease patients [J]. J Biomed Sci. 2017;24(1):43.
3. Thurlow JS, Joshi M, Yan G, et al. Global epidemiology of End-Stage kidney disease and disparities in kidney replacement therapy [J]. Am J Nephrol. 2021;52(2):98–107.
4. Flythe JE, Watnick S. Dialysis for chronic kidney failure: A review [J]. JAMA. 2024;332(18):1559–73.
5. Dixon SJ, Lemberg KM, Lamprecht MR, et al. Ferroptosis: an iron-dependent form of nonapoptotic cell death [J]. Cell. 2012;149(5):1060–72.
6. Dong W, Xu H, Wei W et al. Advances in the study of ferroptosis and its relationship to autoimmune diseases [J]. Int Immunopharmacol. 2024;140:112819.
7. Jing C, Wu Y, Zhang Y, et al. Epigenetic regulation and post-translational modifications of ferroptosis-related factors in cardiovascular diseases [J]. Clin Epigenetics. 2025;17(1):4.
8. Hu W, Liang K, Zhu H et al. Ferroptosis and its role in chronic diseases [J]. Cells. 2022,11(13):2040.
9. Zhang F, Hu Z, Jacob A, et al. An eCIRP inhibitor attenuates fibrosis and ferroptosis in ischemia and reperfusion induced chronic kidney disease [J]. Mol Med. 2025;31(1):11.
10. Luan Y, Huang E, Huang J, et al. Serum myoglobin modulates kidney injury via inducing ferroptosis after exertional heatstroke [J]. J Transl Int Med. 2023;11(2):178–88.
11. Hu Q, Tong Z, Yalikong A, et al. DNAzyme-based faithful probing and pulldown to identify candidate biomarkers of low abundance [J]. Nat Chem. 2024;16(1):122–31.
12. Boschetti E, Righetti PG. Low-Abundance protein enrichment for medical applications: the involvement of combinatorial peptide library technique [J]. Int J Mol Sci. 2023;24(12):10329.
13. Rahman MA, Amirkhani A, Mempin M et al. The Low-Abundance plasma proteome reveals differentially abundant proteins associated with breast implant capsular contracture: A pilot study [J]. Proteomes. 2024;12(3):22.
14. Wang J, Xie W, Sun L, et al. Establishment and clinical application evaluations of a deep mining strategy of plasma proteomics based on nanomaterial protein Coronas [J]. Anal Chim Acta. 2023;1275:341569.
15. Blume JE, Manning WC, Troiano G, et al. Rapid, deep and precise profiling of the plasma proteome with multi-nanoparticle protein Corona. Nat Commun. 2020;11:3662.
16. Szklarczyk D, Nastou K, Koutrouli M, et al. The STRING database in 2025: protein networks with directionality of regulation [J]. Nucleic Acids Res. 2025;53(D1):D730–7.
17. Otasek D, Morris JH, Bouças J, et al. Cytoscape automation: empowering workflow-based network analysis [J]. Genome Biol. 2019;20(1):185.
18. Yoo M, Shin J, Kim J, et al. DSigDB: drug signatures database for gene set analysis [J]. Bioinformatics. 2015;31(18):3069–71.
19. Chen Y, Fang Z-M, Yi X, et al. The interaction between ferroptosis and inflammatory signaling pathways [J]. Cell Death Dis. 2023;14(3):205.
20. Takemura K, Nishi H, Inagi R. Mitochondrial dysfunction in kidney disease and uremic sarcopenia [J]. Front Physiol. 2020;11:565023.
21. Candelaria PV, Leoh LS, Penichet ML et al. Antibodies targeting the transferrin receptor 1 (TfR1) as direct Anti-cancer agents [J]. Front Immunol. 2021;12:607692.
22. Smith CP, Lee WK, Haley M, et al. Proximal tubule transferrin uptake is modulated by cellular iron and mediated by apical membrane megalin-cubilin complex and transferrin receptor 1 [J]. J Biol Chem. 2019;294(17):7025–36.
23. Vermot A, Petit-Härtlein I, Smith SME et al. NADPH oxidases (NOX): an overview from Discovery, molecular mechanisms to physiology and pathology [J]. Antioxid (Basel). 2021; 10(6):890.
24. Negre-Salvayre A, Guerby P, Gayral S, et al. Role of reactive oxygen species in atherosclerosis: lessons from murine genetic models [J]. Free Radic Biol Med. 2020;149:8–22.
25. Singh NK, Rao GN. Emerging role of 12/15-Lipoxygenase (ALOX15) in human pathologies [J]. Prog Lipid Res. 2019;73:28–45.
26. Luo L, Liu K, Deng L, et al. Chicoric acid acts as an ALOX15 inhibitor to prevent ferroptosis in asthma [J]. Int Immunopharmacol. 2024;142(Pt B):113187.
27. Bruna RP, Ludmila F M F C, Márcia R, et al. Uremic toxins and inflammatory profile of patients with chronic kidney disease: A cross-sectional study involving non-dialysis, Hemodialysis and peritoneal Dialysis [J]. Clinical Nutrition ESPEN. 2023;58:491
28. He K, Zhou X, Du H, Zhao J, Deng R, Wang J. A review on the relationship between arachidonic acid 15-Lipoxygenase (ALOX15) and diabetes mellitus. PeerJ. 2023;11:e16239.
29. Singh NK, Rao GN. Emerging role of 12/15-Lipoxygenase (ALOX15) in human pathologies. Prog Lipid Res. 2019;73:28–45.
30. PRNP gene [M]. 2024.
31. Chen X, Kang R, Kroemer G, et al. Organelle-specific regulation of ferroptosis [J]. Cell Death Differ. 2021;28(10):2843–56.
32. Hong J, Li X, Hao Y, et al. The PRMT6/STAT1/ACSL1 axis promotes ferroptosis in diabetic nephropathy [J]. Cell Death Differ. 2024;31(11):1561–75.
33. Joffre J, Wong E, Lawton S, et al. N-Oleoyl dopamine induces IL-10 via central nervous system TRPV1 and improves endotoxemia and sepsis outcomes [J]. J Neuroinflamm. 2022;19(1):118.

34. De Luca R, Mazur K, Kernder A, et al. Mechanisms of N-oleoyldopamine activation of central histaminergic neurons [J]. Neuropharmacology. 2018;143:327–38.
35. Lv J, Song X, Luo Z, et al. Luteolin: exploring its therapeutic potential and molecular mechanisms in pulmonary diseases [J]. Front Pharmacol. 2025;16:1535555.
36. Koufaki M, Theodorou E, Galaris D, et al. Chroman/catechol hybrids: synthesis and evaluation of their activity against oxidative stress-induced cellular damage [J]. J Med Chem. 2006;49(1):300–6.
37. Bi C, Han W, Yu J, et al. Insights into the Pharmacological and therapeutic effects of apigenin in liver injuries and diseases [J]. Heliyon. 2023;9(5):e15609.
38. Siddiquee R, Mahmood T, Ansari VA et al. Apigenin unveiled: an encyclopedic review of its preclinical and clinical insights [J]. Discover Plants. 2025; 2(1):1-24.
39. Thorne AM, Huang H, O'Brien DP, et al. Subclinical effects of remote ischaemic conditioning in human kidney transplants revealed by quantitative proteomics. Clin Proteom. 2020;17(1):39.

Publisher's note